RESEARCH ARTICLE

MICROBIOLOGY

Electrochemical potential enables dormant spores to integrate environmental signals

Kaito Kikuchi[1]†, Leticia Galera-Laporta[1]†, Colleen Weatherwax[1], Jamie Y. Lam[2], Eun Chae Moon[1], Emmanuel A. Theodorakis[2], Jordi Garcia-Ojalvo[3], Gürol M. Süel[1,4,5]*

The dormant state of bacterial spores is generally thought to be devoid of biological activity. We show that despite continued dormancy, spores can integrate environmental signals over time through a preexisting electrochemical potential. Specifically, we studied thousands of individual *Bacillus subtilis* spores that remain dormant when exposed to transient nutrient pulses. Guided by a mathematical model of bacterial electrophysiology, we modulated the decision to exit dormancy by genetically and chemically targeting potassium ion flux. We confirmed that short nutrient pulses result in step-like changes in the electrochemical potential of persistent spores. During dormancy, spores thus gradually release their stored electrochemical potential to integrate extracellular information over time. These findings reveal a decision-making mechanism that operates in physiologically inactive cells.

The formation of bacterial spores (sporulation) is a common and well-characterized survival strategy in many microbial species (*1*, *2*). Spores are partially dehydrated cells enclosed by a protective coat that can survive environmental extremes and remain dormant for years (*3*). They need to be robust to environmental fluctuations to avoid exiting their dormant state (germinating) prematurely. At the same time, spores need to germinate if they detect favorable conditions (*4*) (Fig. 1A). Germination requires the rehydration of the spore, which is promoted by the release of calcium-dipicolinic acid (CaDPA) (*5*). Aside from degradation of RNA immediately after sporulation (*6*), dormant spores appear to have no measurable metabolic or biological activity (*7*). Therefore, it remains unclear whether dormant spores possess any activity that could affect the choice of whether or not to germinate. We thus tested whether dormant *Bacillus subtilis* spores experience any physiological changes in response to subtle environmental signals that do not trigger germination. Addressing these questions could reveal how spores reconcile their robust dormant state with the need to process extracellular information and make an informed decision on whether to continue or exit their dormancy.

Spores can be pretreated with nutrients to promote germination (*8*–*10*). These findings imply that spores can somehow integrate extracellular signals despite their dormancy and thereby alter their future likelihood of triggering germination. Although there are no well-established mechanisms for dormant cells to integrate extracellular information, the ability of spores to modulate their future response suggests a conceptual similarity to a decision-making mechanism in neuroscience known as integrate-and-fire (*11*, *12*). This mechanism describes how neurons respond to small synaptic inputs before reaching the threshold that triggers an action potential (*13*). It is unclear whether dormant spores use a similar mechanism to process environmental inputs and modulate their approach toward a threshold that triggers germination.

Given the physiological inactivity of spores, we investigated a possible integration mechanism based on passive ion flux, which does not require cellular energy. Our findings indicate that physiologically inactive spores integrate environmental signals by modifying preexisting ion gradients that were established during sporulation. Dormant spores can thus use stored electrochemical potential energy to regulate their cell-fate decision without requiring de novo adenosine triphosphate (ATP) synthesis. In this way, spores can alter their distance to the germination threshold depending on environmental inputs while still in the dormant state. This mechanism also reconciles the robust dormancy of spores with the ability to gradually become sensitized to future environmental signals.

Results

B. subtilis *spores can remain dormant despite exposure to germinant pulses*

We confirmed that similar to laboratory strains, undomesticated *B. subtilis* spores can be pretreated with short nutrient (germinant) pulses to increase the likelihood of germination (*8*). Specifically, we imaged spores (Fig. 1B) within a microfluidic device that allows single-cell monitoring and precise control over the components in the incubation medium (materials and methods). We optically tracked the switch in phase-contrast brightness that results from the rehydration of spores during germination (*4*, *14*) (Fig. 1C and fig. S1, A and B). Using this experimental approach, we exposed thousands of spores to a single short germinant pulse [10 mM L-alanine for 3 min] and found that ~95% of spores remained dormant (95.2% ± 1.9%, n = 2244) (Fig. 1D). We used the germinant L-alanine because it is a naturally occurring nutrient that triggers germination through designated receptors in bacterial spores (*15*). Spores that did not germinate upon stimulation remained dormant for at least the next 20 hours of imaging (fig. S1C). Any spore that did germinate in response to the germinant pulse did so on average within 15 min (14.85 ± 1.07, n = 1831) (fig. S1D).

To quantify the integration capacity of spores, we applied a second germinant pulse, which was separated by 2 hours from the first pulse to ensure that germination in response to the first pulse of germinant had subsided. After the second pulse, approximately half of the remaining spores germinated (52.1% ± 6.2%). The germination propensity of spores was independent of their location within the microfluidic chamber (fig. S2). We defined the spore's integration capacity as the population-level change (difference) in the germination probability in response to two consecutive germinant pulses (Fig. 1E). The germination probability increased by 47% ± 1% (mean ± SD, n = 9 replicate populations) between the first and second pulse. Spores thus become sensitized by the first exposure and appear to move closer toward a germination threshold.

A mathematical model of the role of ion flux in responding to germinant pulses

To explain how physiologically inactive spores could integrate information about germinant exposure over time, we explored an ion flux as a mechanism, as this process could occur passively with preexisting ionic gradients established during sporulation. Other processes such as de novo gene expression and enzymatic activity typically require energy, which is highly limited in spores. In particular, we focused here on the flux of potassium because it is the most abundant intracellular ion in bacteria and has physiological roles in the stress response of *B. subtilis* (*16*–*19*). Furthermore, potassium ions have been proposed to stabilize the formation of bacterial spores (*20*). To investigate the possible role of potassium ion flux in dormant spores, we developed a mathematical model based on the Hodgkin–Huxley framework

[1]Molecular Biology Section, Division of Biological Sciences, University of California San Diego, La Jolla, CA 92093, USA. [2]Department of Chemistry and Biochemistry, University of California San Diego, La Jolla, CA 92093, USA. [3]Department of Medicine and Life Sciences, Universitat Pompeu Fabra, 08003 Barcelona, Spain. [4]UCSD Synthetic Biology Institute, University of California San Diego, La Jolla, CA 92093, USA. [5]Center for Microbiome Innovation, University of California San Diego, La Jolla, CA 92093, USA.
*Corresponding author. Email: gsuel@ucsd.edu
†These authors contributed equally to this work.

(*21*) (Fig. 1F, Box 1, and supplementary text). Our model describes how potassium ion flux can drive a spore toward a fixed germination threshold through an integrate-and-fire mechanism, without requiring any physiological activity.

Our mathematical model assumes that potassium ions enter or leave a spore through passive transport through both selective potassium channels and nonspecific ion channels. The direction and rate of potassium flux across the spore membrane depend on the potassium ion concentration gradient, as well as on the membrane potential of the spore (*16*–*19*) (supplementary text). Spores contain high amounts of potassium (*22*, *23*), which would result in ion efflux when channels are open. We assume that ion pumps are inactive during dormancy, given that they require ATP for transport, which is highly limited and not actively produced in spores (*6*). Furthermore, the model assumes that ion channels (both potassium specific and nonspecific) are closed until germinant is added. The channels open in the presence of germinant and close in its absence. Lastly, we assume that the initial potassium content of spores has some variability and that germination begins when a spore's internal potassium concentration drops below a certain value (that is, it reaches the germination threshold) (Fig. 1, G and H). Given these assumptions, the model predicts that, when exposed to consecutive short germinant pulses, few spores germinate during the first pulse, whereas most spores do so during the second or subsequent pulses (Fig. 1I). This increase in the germination probability of spores is consistent with our experimental observations (Fig. 1D). Different germinant concentrations in the first pulse did not markedly change the fraction of germinated spores (fig. S3). By contrast, the germinated fraction increased with higher concentration of L-alanine in the second pulse. This difference in the sensitivity of spores to the first and second germinant pulse concentrations further demonstrates integration of information. The efflux of potassium from dormant spores was also confirmed with an extracellular potassium indicator, Asante Potassium Green-4 tetramethylammonium salt (APG-4 TMA) (fig. S4, A and B). Our modeling approach thus shows how spores might use intracellular potassium concentration to integrate information about previous germinant exposures and change their sensitivity to future exposures.

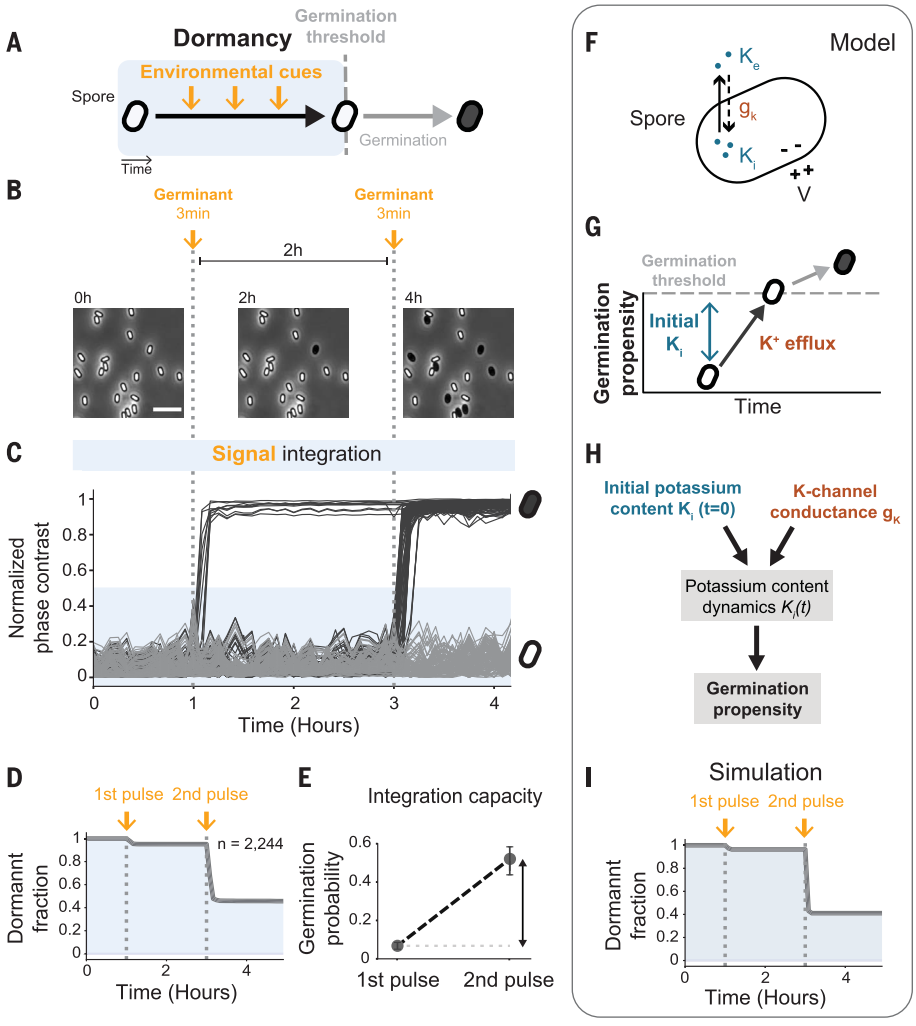

Fig. 1. *B. subtilis* spores integrate over two consecutive germinant pulses. (**A**) Bacterial spores can remain in dormancy (shaded area in blue) for years seemingly without any biological activity. It is thus unclear how spores sense environmental cues while dormant and before triggering germination. (**B**) Filmstrip from phase-contrast microscopy that shows the fractional germination response to the pulses. Spores contained in a microfluidic chip were subjected to 3-min germinant pulses (10 mM L-alanine, dotted vertical lines) separated by 2-hour intervals. These pulses triggered germination of a subset of spores, which was detected by phase-contrast imaging: White dormant spores become phase dark when germinating as they rehydrate. Spores that maintain dormancy despite exposure to germinant pulses provoke the question of whether they can sense and process such environmental information. Scale bar, 5 μm. (**C**) Single-cell time traces showing the change in the normalized phase-contrast intensity during spore germination [n = 200, subset of data from (D)]. Collective fluctuations in the image intensity are due to subtle changes in camera focus. (**D**) Fraction of dormant spores after each germinant pulse (n = 2244). The abrupt decrease in the dormant fraction after the second germinant pulse indicates the ability of spores to integrate signals over consecutive pulses. (**E**) The germination probability in each pulse is calculated based on the remaining dormant spores before each germinant pulse. The difference in the germination probability between the two pulses (vertical arrow) provides a metric to quantify the information integration by spores. (**F**) Cartoon showing the main components of our mathematical model. The flux of potassium in a spore is assumed to depend partially on the difference between its internal (K_i) and external (K_e) concentrations, the K-channel conductance (g_K), and the membrane potential (V) of the spore. (**G**) Spore's approach to the germination threshold is dictated by initial potassium content (K_i) and potassium efflux. (**H**) In the mathematical model, the initial potassium content (K_i, t = 0) and the K-channel conductance (g_K) determine the potassium dynamics in spores [$K_i(t)$]. These dynamics determine the spore's propensity to germinate (see Box 1 and supplementary text). (**I**) Simulated fraction of dormant spores after each germinant pulse.

Initial potassium concentrations define the distance to the germination threshold

Our mathematical model assumes that the initial potassium content defines the distance to the germination threshold (Fig. 1, G and H). To test this, we generated a mutant strain in which the KtrC subunit of the KtrCD potassium importer was deleted, which is expected to lower intracellular potassium content and, consequently, put the spore closer to the threshold compared with wild-type spores (Fig. 2A). KtrC is the major potassium importer expressed in the inner spore membrane during the sporulation process (*24*), which enables potassium uptake (*25*, *26*) (Fig. 2, B and C). By generating spores in the presence of an intracellular potassium indicator, APG-4 acetoxymethyl ester

(AM), we confirmed that the Δ*ktrC* spores contain less potassium than do wild-type spores (fig. S4, C through F). Accordingly, the Δ*ktrC* spores are mathematically predicted to be more likely to germinate in response to the first germinant pulse (Fig. 2D). Indeed, measurements show that 42% of the Δ*ktrC* spores germinated after the first pulse, compared with 5% of the wild-type spores (Fig. 2, E through G, and movie S1). The germinated fraction of Δ*ktrC* spores then further increased after the second pulse (Fig. 2H). We obtained similar results with spores that lacked KtrD, the other subunit of the KtrCD potassium importer (fig. S5A).

Given the high germination probability of Δ*ktrC* spores, almost the entire population (~94%) exited the dormant state after only two germinant pulses (Fig. 2G). However, because the deletion of *ktrC* does not affect potassium efflux in spores, the integration capacity of Δ*ktrC* spores is comparable to that of wild-type spores (Fig. 2I). To further confirm that the lower potassium content of Δ*ktrC* spores caused the higher sensitivity to germinant pulses, we supplied additional potassium during the sporulation of Δ*ktrC* cells. Increasing the potassium content in Δ*ktrC* spores should increase their distance to the germination threshold, which in turn would be reflected in a decrease in their germination probability (fig. S5B). In agreement with those expectations, the addition of 150 mM of potassium in the sporulation medium resulted in Δ*ktrC* spores that responded to germinant pulses similarly to wild-type spores (fig. S5, C and D). These results are consistent with the modeling prediction and support the idea that the initial intracellular potassium concentration of spores specifically defines their distance to the germination threshold.

Potassium ion channels contribute to the integration capacity of spores

We investigated the modeling prediction that spores use potassium efflux to integrate over consecutive germinant pulses. To this end, we studied a mutant strain lacking the YugO potassium ion channel (*27*) (Fig. 3, A and B). We confirmed that Δ*yugO* spores contain less potassium than do wild-type spores with the intracellular potassium indicator APG-4 AM (fig. S4, C through F). Therefore, the Δ*yugO* spores should be initially closer to the germination threshold and be more sensitive than wild-type spores to the first germinant pulse (Fig. 3, A through D). However, the absence of the YugO channel also implies a reduced potassium efflux in response to germinant pulses. According to our model, such reduced potassium efflux in germinant-exposed spores should lower their integration capacity, and thus, the germination probability for subsequent germinant pulses would be lower (Fig. 3D). In other words, the Δ*yugO* spores would not markedly increase their sensitivity to consecutive germinant pulses, which should distinguish this strain from the wild-type and the Δ*ktrC* strains. These mutant spores are therefore predicted to approach the germination threshold more gradually because of reduced potassium efflux.

We experimentally tested these predictions. Essentially, the progression of the wild-type and the Δ*yugO* spores toward the germination threshold are predicted to exhibit a crossover point (Fig. 3D). Experiments confirmed that the Δ*yugO* spores have a higher response than the wild type to the first germinant pulse (with 30% versus 5% of the spores germinating, respectively) (Fig. 3, E, F, and H; movie S2). However, these spores lacked the increase in germination probability in response to subsequent pulses exhibited by the wild-type spores (Fig. 3I). This, in turn, reflects a substantial loss in integration capacity of the Δ*yugO* spores when compared with the wild type (Fig. 3J and fig. S6). The phenotype of the Δ*yugO* spores (high initial germination probability and low integration capacity) is thus consistent with our modeling predictions. Notably, the Δ*yugO* strain also indicates that the reduced efflux of potassium decreases the integration capacity of spores. These results suggest that potassium efflux serves as an integration mechanism that modulates the approach to the germination threshold.

Given the complex phenotype of the Δ*yugO* strain, we turned to chemical perturbations of potassium flux in wild-type spores to independently determine whether potassium flux underlies the integration capacity of spores. We confirmed that modifying the external potassium concentration changed the integration capacity of wild-type spores (fig. S6). Specifically, the absence of potassium in the medium, which we expected to promote higher potassium efflux in spores, increased the integration capacity (from 0.47 ± 0.01 to 0.63 ± 0.02). By contrast, increasing extracellular potassium concentration lowered the integration capacity (Media + 600 mM KCl: 0.32 ± 0.01; Media + 1 M KCl: 0.03 ± 0.01). To test whether reduction in integration capacity might result from increased osmotic stress, we showed that adding 1 M sorbitol had no effect on integration capacity (Media + 1 M sorbitol: 0.44 ± 0.02). The electrochemical gradient of potassium thus influences the integration capacity of spores.

We also tested how the integration capacity of wild-type spores is affected by blocking potassium channels with the drug quinine (1 mM) (Fig. 3, A through C, and figs. S4B and S6) (*28*–*31*). According to our model, such blocking of potassium channels is expected to specifically reduce the germination probability in response to consecutive germinant pulses (Fig. 3D). In agreement with this prediction, treatment of spores with quinine reduced the response of wild-type spores to the second germinant pulse, with around 80% of the spores remaining dormant, in comparison with around 45% in the absence of the drug (Fig. 3, G, H, and I; movie S3). These results support the proposed integrate-and-fire mechanism by showing that similar to the deletion of the YugO channel, chemical blocking of potassium efflux in wild-type spores also impairs their integration capacity (Fig. 3J and fig. S6).

Changes in the electrochemical potential of dormant spores

Our mathematical model proposes that the flux of potassium ions driving the processing of information during dormancy is modulated by the electrochemical potential of the spores. According to the integrate-and-fire mechanism,

Box 1. Mathematical model of dormant spore electrophysiology

According to the processes depicted in Fig. 1F, we assume that the changes in concentrations of extracellular and intracellular potassium—K_e and K_i, respectively—are governed by the flow of potassium ions through the spore membrane:

$$\frac{dK_e}{dt} = Fg_K n^4(V - V_K) + Fg_n n^4(V - V_n) - \gamma_e(K_e - K_m)$$
$$\frac{dK_i}{dt} = -Fg_K n^4(V - V_K) - Fg_n n^4(V - V_n)$$

The model includes ion flow through both specific and nonspecific channels, with conductances g_K and g_n, respectively. Additionally, extracellular potassium is subject to a relaxational term (third term in the right-hand side of the K_e equation) that pulls it to the concentration of potassium in the medium, K_m. Ion flow through the channels depends on the electrochemical state of the spore, given by its membrane potential V and reversal potentials V_K and V_n, which correspond to specific and nonspecific ions, respectively. Crucially, the reversal potential of potassium depends on the potassium concentrations through the Nernst equation:

$$V_K = V_{K0} \ln(K_e/K_i)$$

As mentioned in the main text, the channels are assumed to open in the presence of germinant, which produces an outward flux of potassium and consequently a sudden increase in membrane potential. The dynamics of the membrane potential V and gating variable n are described in the supplementary text, together with the rest of the parameters and all parameter values.

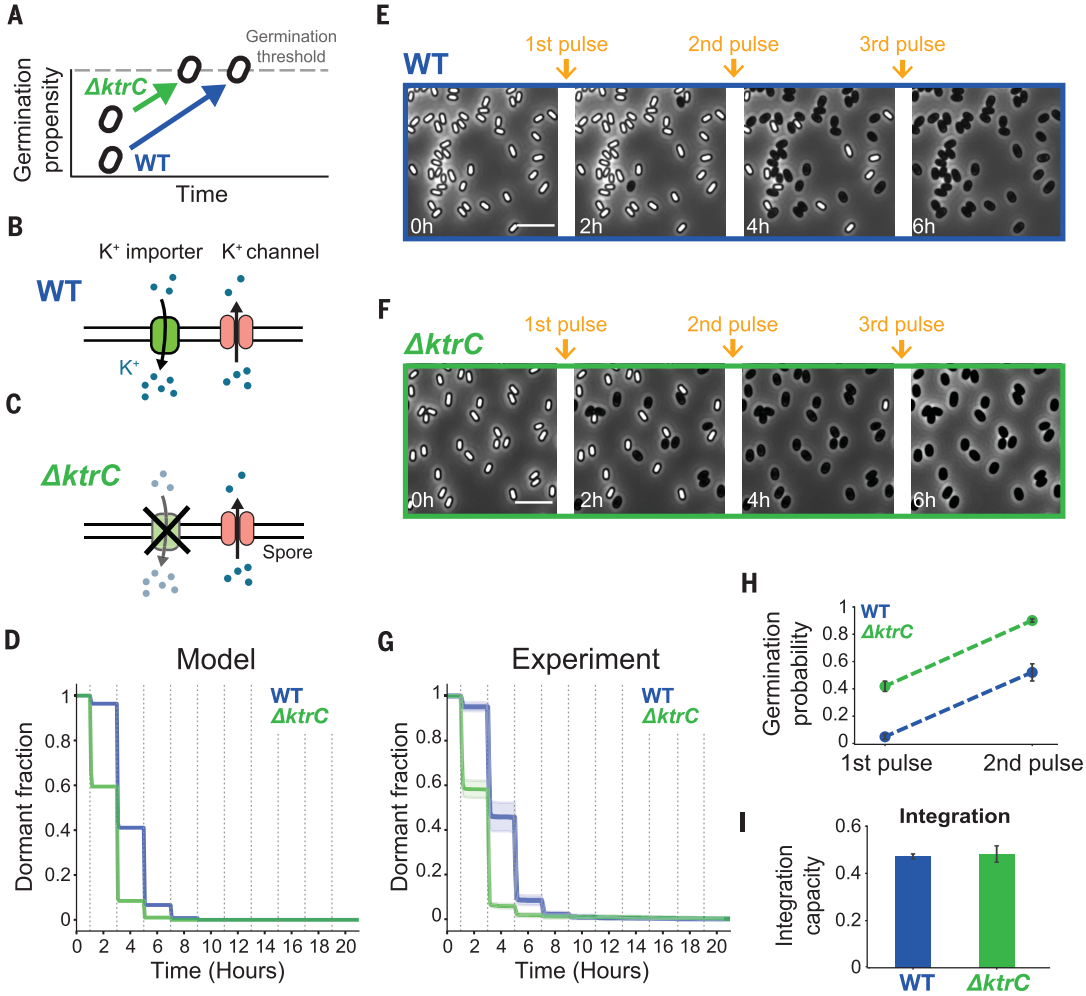

Fig. 2. Role of potassium in the germination threshold. (**A**) Model predicts that the deletion of the KtrC importer reduces the distance of spores to their germination threshold. This, in turn, will increase the germination propensity of Δ*ktrC* spores compared with wild-type (WT) spores. (**B**) WT cells contain both potassium importers and ion channels. (**C**) The *ktrC* mutant spores (Δ*ktrC*) lack the gene for the potassium importer KtrC. (**D**) Model-generated dormant fraction of the WT (blue), and the Δ*ktrC* (green) strains. Dotted vertical lines indicate germinant pulses. (**E** and **F**) Phase-contrast microscopy filmstrips for representative WT (E) and Δ*ktrC* spores (F), respectively. Snapshots show spores before and after the indicated germinant pulses. Scale bars, 5 μm. (**G**) Dormant fraction from single-cell experimental results for WT (blue, mean ± SD, n = 2244, data from Fig. 1D) and Δ*ktrC* (green, mean ± SD, n = 2154). Dotted vertical lines indicate germinant pulses. (**H**) Germination probabilities of the WT and the Δ*ktrC* spores increase with consecutive pulses. Both strains reach 50% germination out of all initial spores (half-maximum germination) after two consecutive pulses. Error bars represent standard deviation. (**I**) Bar plot showing the integration capacity of the WT and the Δ*ktrC* strains (0.47 ± 0.01 and 0.48 ± 0.03, respectively) calculated from the differences in germination probabilities shown in (H). Error bars represent standard deviation.

spores that are further from their germination threshold would require multiple germinant pulses to reach the threshold, each pulse causing an incremental electrochemical potential change (Fig. 4A). Specifically, the transient efflux of potassium cations triggered by germinant pulses is mathematically predicted to increase the negative electrochemical potential of spores in a step-like manner, even when the pulses do not trigger germination (Fig. 4B). To test this prediction, we used a previously characterized cationic fluorescent dye, thioflavin-T (ThT) to measure changes in the electrochemical potential of dormant spores (materials and methods) (*16*, *32*). As spores are notoriously impermeable to most chemicals (*33*), we expected that peripheral staining by ThT would reflect the spore's overall negative electrochemical potential (*20*).

To experimentally test our modeling prediction of electrochemical potential jumps, we tracked thousands of individual wild-type spores over time and simultaneously imaged phase-contrast and ThT fluorescence intensities (Fig. 4, C through F). Spores that did not trigger germination exhibited sudden changes in their electrochemical potential in response to germinant pulses (movie S4). Spores that required multiple germinant pulses to trigger germination exhibited a multistep progression before reaching their germination threshold. These increases in the ThT signal were not due to increased spore permeability, as ThT continued to stain the spore's periphery and did not transition to its interior (Fig. 4D and movie S4). Therefore, accumulation of ThT on the spore periphery appears to reflect changes in the ionic content of the spore. We observed no characteristic changes of the phase-contrast brightness of dormant spores during the increases in the ThT signal (fig. S7A). We also tested L-valine, another naturally occurring germinant (*34*), and observed similar changes in ThT signal (fig. S7B). Furthermore, we used another positively charged dye, tetramethylrhodamine methyl ester (TMRM), which is commonly used to measure the electrochemical potential of cells (*35*). TMRM also stained the periphery of spores, and increases in the TMRM signal amplitude were qualitatively similar to those measured with ThT (fig. S8, A and B). To validate that the observed jumps in fluorescence during germinant additions were not simply a staining artifact, we synthesized a charge-neutral version of ThT (Fig. 4E, inset; figs. S8, C and D, and S9; materials and methods; and supplementary text). Although this charge-neutral ThT dye also stained the spore periphery, we observed no increases in the signal amplitude during germinant pulses. Instead, the fluorescence signal of the neutral ThT dye monotonically decayed over time, which was likely due to photobleaching. To exclude the possibility that the observed changes in electrochemical potential could be related to the release of CaDPA during the initiation of germination, we generated a mutant strain that lacked a subunit of the SpoVA channel, namely SpoVAF (fig. S10A). This subunit is

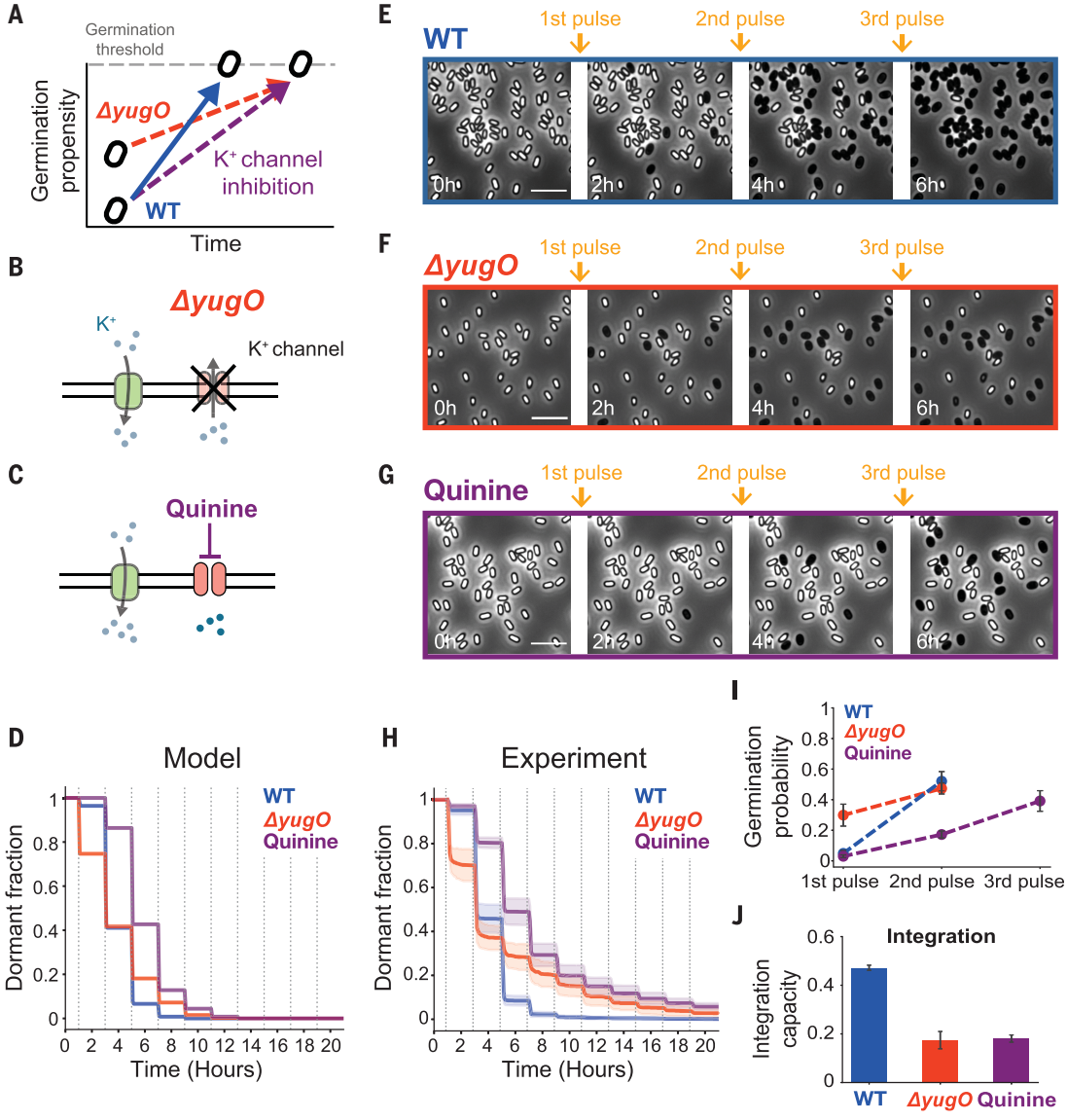

Fig. 3. Potassium ion flux underlies integration capacity of dormant spores. (**A**) Δ*yugO* mutant spores are expected to be initially closer to the germination threshold but have slower potassium efflux, which affects their approach to the threshold. The inhibition of potassium channels in WT spores is similarly expected to affect their approach to the germination threshold. (**B**) Δ*yugO* mutant spores lack the gene for the YugO channel, which is the only known potassium-specific channel in *B. subtilis* spores. (**C**) Quinine targets potassium channels, which blocks ion efflux. (**D**) Model-generated dormant fraction of WT (blue), Δ*yugO* (red), and quinine addition to WT spores (purple). (**E** to **G**) Filmstrips for representative WT (E) and Δ*yugO* (F) spores and WT spores in the presence of 1 mM quinine (G), respectively. Snapshots show spores before and after the indicated germinant pulses. Scale bars, 5 μm. (**H**) Dormant fraction from single-cell measurements of WT (mean ± SD; blue, n = 2244, data from Fig. 1D), Δ*yugO* (mean ± SD; red, n = 1058), and 1 mM quinine addition to WT spores (mean ± SD, purple, n = 4491). (**I**) Germination probability until half-maximum germination for WT (data from Fig. 2H), Δ*yugO*, and quinine addition. The inhibition of potassium efflux reduces the germination probability, requiring three pulses to reach the half-maximum germination. Error bars represent standard deviation. (**J**) Genetic and chemical inhibition of potassium efflux (Δ*yugO* and quinine addition, respectively) reduces the integration capacity of spores (WT 0.47 ± 0.01, data from Fig. 2I, Δ*yugO* 0.17 ± 0.04, and quinine 0.18 ± 0.01; mean ± SD).

essential for effective CaDPA release during germination, and its deletion causes a delay in germination (*36*). The deletion of SpoVAF slowed the response time of spores to L-alanine (fig. S10B). However, loss of *spoVAF* did not affect the electrochemical potential changes that we observed in spores (fig. S10, C and D), which indicates that CaDPA release is not required for the integration of information in dormant spores. Together, these results demonstrate that germinant pulses cause sudden changes in the electrochemical potential of spores that otherwise remain dormant. As predicted, spores that required multiple germinant pulses to initiate germination also exhibited multiple jumps in their electrochemical potential, which indicates their greater distance to the germination threshold. The ability to visualize and observe a multistep and gradual approach of dormant spores toward their germination threshold provides further evidence in support of the integrate-and-fire mechanism.

We investigated whether the integration capacity that we determined from population-level statistics correlated with the independently observed jumps in the electrochemical potential of individual spores. In particular, a higher integration capacity should correlate with a higher change in electrochemical potential. We therefore measured germinant-induced changes in the electrochemical potential for thousands of spores obtained from various perturbations considered in this study (Fig. 4, F and G). Higher integration capacity correlated with a higher average increase in electrochemical potential (Fig. 4H). Specifically, wild-type and Δ*ktrC* spores, which have similarly high changes in electrochemical potential, also exhibited relatively higher integration capacities. Furthermore, the Δ*yugO* and the quinine-exposed wild-type spores, which both exhibited lower average changes in their electrochemical potential, had reduced integration capacities. These findings support the prediction that dormant spores integrate environmental information through ion flux-induced changes in their electrochemical potential.

Discussion

We studied how physiologically inactive spores detect and respond to transient germinant pulses.

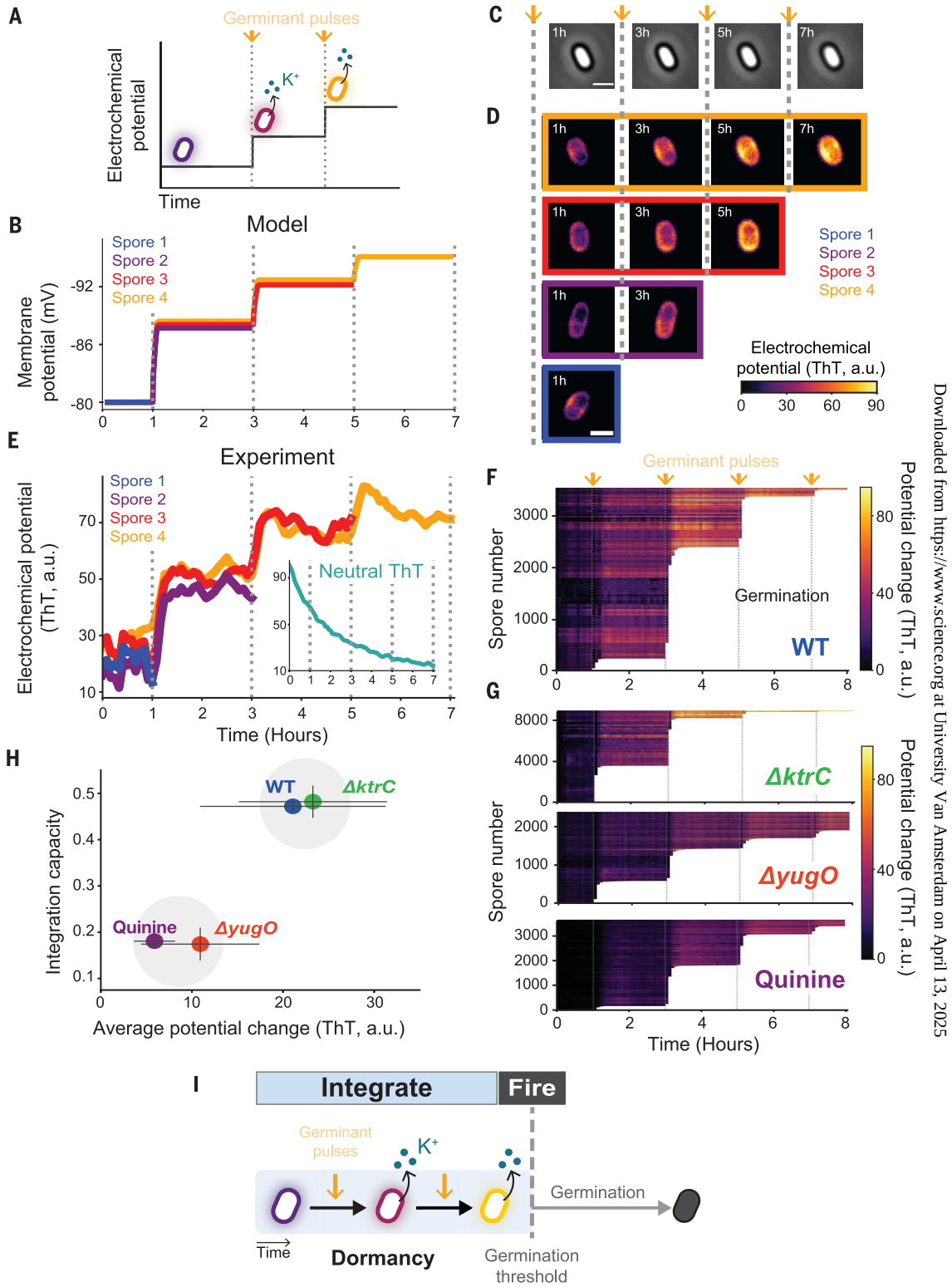

Fig. 4. Dormant spores exhibit sudden changes in their electrochemical potential, visualizing integration over germinant pulses. (**A**) Cartoon illustrating the hypothesis that spores release potassium after each germinant pulse, generating a change in their electrochemical potential. (**B**) Mathematically predicted stepwise membrane potential (mV) jumps when spores are exposed to germinant pulses (dotted vertical lines). Depicted are representative time traces for individual spores that germinate in response to different germinant pulse numbers. The termination of the time trace indicates germination. (**C**) Phase-contrast images of a spore that remains dormant (phase bright) despite exposure to three consecutive germinant pulses. Dotted vertical lines indicate germinant pulse exposure. Scale bar, 1 μm. (**D**) Top fluorescence filmstrip shows the color-coded electrochemical potential amplitude [ThT, arbitrary units (a.u.)] of the spore depicted in (C). The other three filmstrips below show individual spores, each of which germinate in response to different germinant pulses. (**E**) Single-cell time traces of the electrochemical potential signal (ThT, a.u.) for the corresponding spores in Fig. 3D (see fig. S7A for corresponding phase-contrast traces). The termination of the time traces indicates germination. The inset shows the time trace of a single spore stained with the charge-neutral ThT fluorescent dye (see fig. S8D for data from multiple spores). (**F**) Measurement of 3484 individual WT spores showing amplitude color-coded time traces that show the changes in electrochemical potential signal (ThT, a.u.) triggered by germinant pulses (dotted vertical lines). The termination of the time trace (white region) indicates germination. (**G**) Single-cell time traces of the potential change (ThT, a.u) for Δ*ktrC* (n = 8790), Δ*yugO* (n = 2380), and WT with 1 mM quinine (n = 3653), respectively. Each line represents a single-spore time trace until germination (white region). Germinant pulses are indicated with arrows and dotted vertical lines. (**H**) Scatter plot of the integration capacity as a function of the average potential change (ThT, a.u) of all strains and conditions tested in this study: WT, Δ*ktrC*, Δ*yugO*, and WT with quinine. (**I**) Conceptual summary of the proposed integrate-and-fire mechanism. Spores integrate germinant exposure information over time through efflux of potassium ions. The resulting change in electrochemical potential drives them toward a germination threshold. Spores that reach the threshold "fire" the germination program, which is marked by the abrupt change in phase-contrast refractility.

Our results reveal that despite their dormancy, spores can integrate extracellular information and alter their intrinsic state. This ability to process information appears to be supported by preexisting ionic gradients generated during sporulation. In this way, dormant spores can reach the decision to initiate germination by using electrochemical potential energy, rather than requiring a source of cellular energy, such as ATP. Spores may thus be analogous to a biological capacitor in that they store and use an electrochemical potential to move closer to the germination threshold (Fig. 4I). The integrate-and-fire model proposed here provides both a conceptual and mechanistic explanation for how spores can respond to an environmental signal despite being physiologically inactive. The ability to sum inputs over time before reaching a threshold ensures that germination is triggered only when favorable conditions persist while ignoring small environmental fluctuations. Although the integrate-and-fire model is used to describe how neurons process information, our work suggests that this concept may represent a more general solution to the need for information processing in diverse biological systems, including energy-limited cells.

REFERENCES AND NOTES

1. P. Stragier, R. Losick, *Annu. Rev. Genet.* **30**, 297–41 (1996).
2. P. J. Piggot, D. W. Hilbert, *Curr. Opin. Microbiol.* **7**, 579–586 (2004).
3. M. Huang, C. M. Hull, *Curr. Genet.* **63**, 831–838 (2017).
4. R. Pandey *et al*., *PLOS ONE* **8**, e58972 (2013).
5. S. Wang, P. Setlow, Y. Q. Li, *J. Bacteriol.* **197**, 1095–1103 (2015).
6. P. Setlow, G. Christie, *Front. Microbiol.* **11**, 596092 (2020).
7. S. Ghosh, G. Korza, M. Maciejewski, P. Setlow, *J. Bacteriol.* **197**, 992–1001 (2015).
8. S. Wang, J. R. Faeder, P. Setlow, Y. Q. Li, *mBio* **6**, e01859–e15 (2015).
9. P. Zhang, J. Liang, X. Yi, P. Setlow, Y. Q. Li, *J. Bacteriol.* **196**, 2443–2454 (2014).
10. L. V. Pedrero-López, B. Pérez-García, K. Mehltreter, M. E. Sánchez-Coronado, A. Orozco-Segovia, *J. Plant Physiol.* **232**, 284–290 (2019).
11. N. Brunel, M. C. W. van Rossum, *Biol. Cybern.* **97**, 337–339 (2007).
12. H. C. Tuckwell, *Introduction to Theoretical Neurobiology* (Cambridge Studies in Mathematical Biology, Cambridge University Press, 1988).
13. A. N. Burkitt, *Biol. Cybern.* **95**, 1–19 (2006).
14. P. Setlow, *J. Bacteriol.* **196**, 1297–1305 (2014).
15. A. Moir, G. Cooper, *Microbiol. Spectr.* 10.1128/microbiolspec.TBS-0014-2012, (2015).
16. A. Prindle *et al*., *Nature* **527**, 59–63 (2015).
17. J. W. Larkin *et al*., *Cell Syst.* **7**, 137–145.e3 (2018).
18. C.-Y. Yang *et al*., *Cell Syst.* **10**, 417–423.e3 (2020).
19. J. Humphries *et al*., *Cell* **168**, 200–209.e12 (2017).
20. T. Sirec, J. M. Benarroch, P. Buffard, J. Garcia-Ojalvo, M. Asally, *iScience* **16**, 378–389 (2019).
21. A. L. Hodgkin, A. F. Huxley, *J. Physiol.* **117**, 500–544 (1952).
22. E. Eisenstadt, *J. Bacteriol.* **112**, 264–267 (1972).
23. A. M. Whatmore, J. A. Chudek, R. H. Reed, *J. Gen. Microbiol.* **136**, 2527–2535 (1990).
24. L. Zheng *et al*., *J. Proteome Res.* **15**, 585–594 (2016).
25. G. Holtmann, E. P. Bakker, N. Uozumi, E. Bremer, *J. Bacteriol.* **185**, 1289–1298 (2003).
26. J. Stautz *et al*., *J. Mol. Biol.* **433**, 166968 (2021).
27. M. E. Lundberg, E. C. Becker, S. Choe, *PLOS ONE* **8**, e60993 (2013).
28. J. P. Barfield, C. H. Yeung, T. G. Cooper, *Mol. Hum. Reprod.* **11**, 891–897 (2005).
29. D. E. Cortezzo, B. Setlow, P. Setlow, *J. Appl. Microbiol.* **96**, 725–741 (2004).
30. E. Mancilla, E. Rojas, *FEBS Lett.* **260**, 105–108 (1990).
31. C. Mitchell, J. F. Skomurski, J. C. Vary, *FEMS Microbiol. Lett.* **34**, 211–214 (1986).
32. D. D. Lee *et al*., *Cell* **177**, 352–360.e13 (2019).
33. A. E. Cowan *et al*., *Proc. Natl. Acad. Sci. U.S.A.* **101**, 7733–7738 (2004).
34. A. Moir, D. A. Smith, *Annu. Rev. Microbiol.* **44**, 531–553 (1990).
35. A. P. Leonard *et al*., *Biochim. Biophys. Acta* **1853**, 348–360 (2015).
36. A. Perez-Valdespino *et al*., *J. Bacteriol.* **196**, 2077–2088 (2014).
37. K. Kikuchi *et al*., Electrochemical potential enables dormant spores to integrate environmental signals. Version 1, Zenodo (2022); https://doi.org/10.5281/zenodo.6967596.

ACKNOWLEDGMENTS

We acknowledge M. Asally, T. Çağatay, J. Larkin, C. Comerci, and K. Süel for helpful discussions; W. Winkler and D. Kearns for kindly providing bacterial strains; and J. Humphries for help with strain construction. **Funding:** National Institute of General Medical Sciences (grant R01 GM121888 to G.M.S.); National Institute of General Medical Sciences (grant R35 GM139645 to G.M.S.); Howard Hughes Medical Institute-Simons Foundation Faculty Scholars Program (G.M.S.); U.S. Army Research Office (W911NF2210107); Defense Advanced Research Projects Agency (HR0011-21-C-0192); Spanish Ministry of Science, Innovation and Universities (Project PGC2018-101251-B-I00 to J.G.O.); FEDER (CEX2018-000792-M to J.G.O.); Generalitat de Catalunya ICREA Academia program (J.G.O.); ANRI Fellowship (K.K.); and National Institute on Aging (grant RF1 AG062362 to E.A.T.). **Author contributions:** Conceptualization: K.K., L.G.L., C.W., J.G.O., and G.M.S.; Methodology: K.K., L.G.L., C.W., J.G.O., and G.M.S.; Experiments: L.G.L., K.K., and E.C.M.; Design, synthesis, and characterization of the charge-neutral version of ThT: J.Y.L. and E.A.T.; Experimental data analysis: K.K., L.G.L., and E.C.M.; Mathematical modeling: C.W. and J.G.O.; Funding acquisition: G.M.S., J.G.O., and E.A.T.; Supervision: G.M.S., J.G.O., and E.A.T.; Project administration: G.M.S.; Writing: G.M.S., K.K., L.G.L., C.W., J.G.O., E.C.M., J.Y.L., and E.A.T. **Competing interests:** The authors declare that they have no competing interests. **Data and materials availability:** All data are available in the manuscript or the supplementary material. All bacterial strains and material generated in this study are available from the authors. Code for the mathematical model and for generating the germination cumulative density functions are available at https://github.com/suellab/Kikuchi_Galera-Laporta_2022 and Zenodo (*37*).

SUPPLEMENTARY MATERIALS

science.org/doi/10.1126/science.abl7484
Materials and Methods
Supplementary Text
Figs. S1 to S10
References (*38*–*50*)
MDAR Reproducibility Checklist
Movies S1 to S4

Submitted 2 August 2021; resubmitted 9 February 2022
Accepted 9 August 2022
10.1126/science.abl7484